

International Journal of Modern Physics D
 © World Scientific Publishing Company

A theoretical calculation of microlensing signatures caused by free-floating planets towards the Galactic bulge

L. HAMOLLI, M. HAFIZI

Department of Physics, University of Tirana, Albania

A.A. NUCITA

Department of Mathematics and Physics Ennio De Giorgi and INFN, University of Salento, CP 193, I-73100 Lecce, Italy

Received (received date)

Revised (revised date)

Free-floating planets are recently drawing a special interest of the scientific community. Gravitational microlensing is up to now the exclusive method for the investigation of free-floating planets, including their spatial distribution function and mass function. In this work, we examine the possibility that the future Euclid space-based observatory may allow to discover a substantial number of microlensing events caused by free-floating planets. Based on latest results about the free-floating planet mass function in the mass range $[10^{-5}, 10^{-2}]M_{\odot}$, we calculate the optical depth towards the Galactic bulge as well as the expected microlensing rate and find that Euclid may be able to detect hundreds to thousands of these events per month. Making use of a synthetic population, we also investigate the possibility of detecting parallax effect in simulated microlensing events due to free-floating planets and find a significant efficiency for the parallax detection that turns out to be around 30%.

1. Introduction

Gravitational microlensing is at present the only observational technique that allows the detection of extremely faint or even completely dark objects, when their gravitational field acts as a lens to magnify background source stars¹. A gravitational lens is characterized by its Einstein ring radius,

$$R_E(M, x) = \sqrt{\frac{4GM D_s}{c^2} x(1-x)}, \quad (1)$$

which is the radius of the ring image formed when the observer, the lens and the source are perfectly aligned. Here M is the mass of the lens and $x = D_l/D_s$ is the normalized lens distance, whereas D_s and D_l are the source-observer and lens-observer distance, respectively.

In a microlensing event, the image separation is too small to be resolved and the observable feature is the variation in time of the light magnification, as due to

the lens-source relative motion. The key parameter of the microlensing light curve is the Einstein radius crossing time given by

$$T_E = \frac{R_E}{v_T}, \quad (2)$$

where v_T is the relative transverse velocity between the lens and the source.

In the simplest case (named standard case), when both the lens and the source can be considered as point-like objects and, additionally, their relative motion with respect to the observer is assumed to be linear, the amplification of the source star follows the Paczyński profile ¹

$$A_s = \frac{u^2(t) + 2}{u(t)\sqrt{u^2(t) + 4}}, \quad (3)$$

where

$$u(t) = \sqrt{u_0^2 + \left(\frac{t - t_0}{t_E}\right)^2}, \quad (4)$$

is the separation between the lens and the line of sight in units of R_E and u_0 is the minimum separation (impact parameter) obtained at the moment of the peak magnification t_0 . The light curve obtained by equation (3) is, evidently, symmetric around t_0 .

When the projected source encounters the Einstein ring of the lens, i.e. when the projected separation is $u = 1$, the source amplification takes a specific value defined as the threshold amplification $A_{th} = 1.34$. For space-based telescopes, due to the absence of seeing effects, the amplification threshold may be much smaller than 1.34, with a corresponding much larger value for the impact parameter. For $A_{th} = 1.001$, as expected for the Euclid telescope, the maximum value of u in equation (3) turns out to be $u_{max} = 6.54$.

A standard microlensing light curve is described by three parameters, t_0 , t_E and u_0 , but only one of them, the Einstein radius crossing time, t_E , contains information about the lens. As can be seen from equations (1) and (2), the event duration is determined by three unknown parameters of the lens: its mass M , the transverse velocity v_T and the distance D_l . There are several methods that have been proposed for breaking the microlensing parameter degeneracy. Among them there is the parallax effects, occurring due to the motion of the Earth around the Sun and the effect of the relative accelerations among the observer, the lens and the source ². These second order effects induce small deviations in the light curve (with respect to the Paczyński profile), which may be extremely useful to break, at least partially, the parameter degeneracy problem in microlensing observations.

Recently, it has been reported the observation by MOA-II of a galactic population of free objects with planetary masses, named free-floating planets (FFPs) ³. Due to the intrinsic faintness of the FFPs, it is very hard to observe them directly. Hence, the gravitational microlensing method may be a suitable technique to detect such objects when they act as lenses for the background stars. Of course, as it will

be clarified in the following, the small planetary masses imply microlensing events with very short time-scales.

The purpose of this paper is the investigation of the traces of FFPs, among other galactic lens populations, in microlensing events that might be observed serendipitously during the planned observations of the Euclid satellite towards the Galactic bulge. In Section 2, we discuss the FFP mass function, their spatial distribution and the adopted velocity distribution. In Section 3, we review the microlensing method and its parameters in the case of Euclid observations. In Section 4, we show how the parallax effect may help in solving, at least partially, the degeneracy of parameters in the microlensing curves. Our main results are presented and discussed in Section 5, while in Section 6 we draw the main conclusions of this work.

2. Planetary population

In a recent survey of the Galactic bulge, the MOA-II collaboration³ reported the discovery of planetary-mass objects either very distant from their host stars (more than 100 AU away) or entirely unbound. By analyzing the timescale distribution of all the observed microlensing events, they found a statistically significant excess of events with timescale $t < 2$ days as compared to the number of expected events from the standard Galactic model. The stellar mass-function for the standard Galactic model is generally expressed, for stars with mass $\leq 1M_{\odot}$ and brown dwarfs (BDs), with three power laws of the form

$$\frac{dN}{dM} \sim M^{-\alpha_i} \quad \begin{cases} \alpha_1 = 2 & 0.7M_{\odot} < M < M_{\odot} \\ \alpha_2 = 1.3 & 0.08M_{\odot} < M < 0.7M_{\odot} \\ \alpha_{BD} = 0.49_{-0.27}^{+0.24} & 0.01M_{\odot} < M < 0.08M_{\odot}, \end{cases} \quad (5)$$

A best-fit procedure to the observed microlensing events due to FFPs has also allowed Sumi et al.³ to extend and constrain the power-law mass function at the low-mass regime of the FFPs

$$\frac{dN}{dM} = k_{PL} M^{-\alpha_{PL}}, \quad \alpha_{PL} = 1.3_{-0.4}^{+0.3}, \quad 10^{-5}M_{\odot} < M < 10^{-2}M_{\odot}. \quad (6)$$

The derived number of planetary mass objects per star turns out to be very large, although rather poorly constrained: $N_{PL} = 5.5_{-4.3}^{+18.1}$, mainly due to the poor precision of the lens mass estimate below $10^{-4}M_{\odot}$.

The abrupt change from $\alpha_{BD} = 0.49$ to $\alpha_{PL} = 1.3$ favors the idea of a separate population, whose formation process is different from that of stars and BDs. These objects may have formed in proto-planetary disks and subsequently scattered into unbound or very distant orbits, becoming FFPs.

From the likelihood contours of the power-law indices found in the brown dwarf and planetary-mass regime³, we get a useful correlation between α_{BD} and α_{PL}

$$\alpha_{BD} = 1.7 - \alpha_{PL}. \quad (7)$$

Regarding the spatial distribution of the FFPs, we assume that they are distributed as the stars in the Milky way^{4,5,6}. Hence, we considered the following

4

density distributions:

1. exponential thin disk,

$$\rho(R, z) = \rho_0^{\text{Dthin}}(M) e^{-|z|/H} e^{-(R-R_0)/h}, \quad (8)$$

in cylindrical coordinates R (the galactocentric distance in the galactic plane) and z (the distance from the galactic plane). The scale parameters are $H \sim 0.30$ kpc, $h \sim 3.5$ kpc; $R_0 = 8.5$ kpc is the local galactocentric distance.

2. exponential thick disk,

$$\rho(R, z) = \rho_0^{\text{Dthick}}(M) e^{-|z|/H} e^{-(R-R_0)/h}, \quad (9)$$

with $H \sim 1$ kpc, $h \sim 3.5$ kpc and $R_0 = 8.5$ kpc.

3. triaxial bulge^{5,6,7}

$$\rho(x, y, z) = \rho_0^{\text{Bulge}}(M) e^{-s^2/2}, \quad \text{with } s^4 = (x^2/a^2 + y^2/b^2)^2 + z^4/c^4, \quad (10)$$

where $a = 1.49$ kpc, $b = 0.58$ kpc, $c = 0.40$ kpc.

For the FFP velocity distribution, we assume for each coordinate the Maxwellian distribution^{8,9}

$$f(v_i) \propto \exp\left[-\frac{(v_i - \bar{v}_i)^2}{2\sigma_i^2}\right], \quad i \in \{x, y, z\}, \quad (11)$$

where the coordinates (x, y, z) have their origin at the galactic center and the x and z -axes point to the Sun and the north Galactic pole, respectively. We are interested only to the perpendicular velocity with respect to the line of sight, namely to y and z components. For lenses in the Galactic bulge we use the mean velocity components $\bar{v}_y = \bar{v}_z = 0$, with dispersion $\sigma_y = \sigma_z = 100$ km/s; for lenses in the Galactic disk we use the mean velocity components $\bar{v}_y = 220$ km/s, $\bar{v}_z = 0$, with dispersion velocity $\sigma_y = \sigma_z = 30$ km/s for the thin disk and $\sigma_y = \sigma_z = 50$ km/s for the thick disk.

3. Microlensing events towards the Galactic bulge

Several microlensing surveys with relatively high image sampling have been undertaken until now towards the Galactic bulge by the MOA (Microlensing Observations in Astrophysics) Collaboration¹⁰ and the OGLE (Optical Gravitational Lensing Experiment) Collaboration¹¹ (to cite only some of them), with the aim of searching for MACHOs (Massive Astrophysical Compact Halo Objects) and exoplanets. These surveys (undertaken since about two decades) have allowed the detection of several thousands of microlensing events, most of which are due to self-lensing (stars either in the Galactic disk and bulge). Ground-based observations may detect low-mass lenses (short time duration events) only with great difficulties, so to search for lens masses below $0.01M_\odot$, as for FFPs, space-based observations are needed. At present, there are two space-based missions which are planned for detecting microlensing events towards the Galactic bulge: the Wide-Field Infrared Survey Telescope (WFIRST) and Euclid.

Euclid is a Medium Class mission of the ESA (European Space Agency), which is scheduled to be launched in 2017. For ten months, not necessarily consecutive¹², it will perform microlensing observations towards the Galactic bulge. The galactic coordinates of the Euclid line of sight are $b = -1.7^\circ$, $l = 1.1^\circ$, the distance of observation can be considered $D_s = (7 - 10)$ kpc, with mean value at $D_s = 8.5$ kpc and the observing image rate (cadence) is expected to be about 20 min.

In order to study the expected microlensing events that may be detected by the Euclid observatory we start by evaluating the microlensing optical depth and the event rate. The microlensing optical depth is defined as the probability that at any time a random star is magnified more than the threshold amplification $A_{th} = 1.34$ by a lens belonging to a given population of lenses. It is given by (see e.g. ^{13,14})

$$\tau = \int_0^{D_s} n(D_l) \pi R_E^2 dD_l = \frac{4\pi G D_s^2}{c^2} \int_0^1 \rho(M, x) x(1-x) dx, \quad (12)$$

where $\rho(M, x)$ is the mass density of the lens population; $x = D_l/D_s$.

The microlensing rate is the number of events per unit time and per monitored star due to the lens population. It is given by (see e.g. ^{13,14})

$$\Gamma = \int \frac{n(x) f(\mathbf{v}_l - \mathbf{v}_t) f(\mathbf{v}_s) dx d\mathbf{v}_l d\mathbf{v}_s}{dt}, \quad (13)$$

where \mathbf{v}_l , \mathbf{v}_s and \mathbf{v}_t are the lens, the source and the microlensing tube two-velocities in the plane transverse to the line of sight. The velocity distribution functions $f(\mathbf{v}_l)$ and $f(\mathbf{v}_s)$ are assumed to have Maxwellian forms^{8,9}, with one-dimensional dispersion velocities different for each lens and source population. The tube velocity is given by

$$v_t^2(x) = (1-x)^2 v_\odot^2 + x^2 v_s^2 + 2x(1-x) v_\odot v_s \cos \theta, \quad (14)$$

where \mathbf{v}_\odot is the local velocity transverse to the line of sight and θ is the angle between \mathbf{v}_\odot and \mathbf{v}_s .

In the case of observations towards the Galactic bulge, the source stars are mostly bulge stars which are distributed following, as usual, the same triaxial mass density model as given in eq. (10) with $\rho_0^{\text{Bulge}} = M_b / (8\pi abc)$, where $M_b \simeq 2 \times 10^{10} M_\odot$, $a = 1.49$ kpc, $b = 0.58$ kpc and $c = 0.40$ kpc.

The limiting line flux of Euclid Telescope is estimated to be $F_l = 3 \times 10^{-19} J_s^{-1} m^{-2}$,¹² whereas the flux of a Sun-like star situated at the Galactic center is $F_\odot = 4.44 \times 10^{-16} J_s^{-1} m^{-2}$. Based on the mass-luminosity relation $\frac{L}{L_\odot} = \left(\frac{M}{M_\odot}\right)^{2.4}$ for low-mass stars ($M < 0.8 M_\odot$), it can be directly shown that the telescope can observe all bulge stars.

The mean mass for bulge stars is $\langle M \rangle = 0.27 M_\odot$, found by using the Salpeter mass function¹⁵ $\frac{dN}{dM} \sim M^{-2.4}$; the Euclid's field of view is 0.54 square degree, hence the number of source stars in Euclid microlensing observations will be $N_{ED} = 2.3 \times 10^8$. This number has to be multiplied by the microlensing rate (13) and the time of observation (in the following we take $t_{\text{obs}} = 1$ month) to get an estimate of the number of microlensing event that we expect to be detectable

6

by the Euclid telescope.

4. Parallax effect

The parallax effect due to the motion of the Earth around the Sun may leave in microlensing events some observable feature which can be used to break the degeneracy of microlensing parameters, or at least to constrain the microlensing parameter space. Here, we are focusing on the investigation of the parallax traces left on microlensing events that will possibly be detected by the Euclid telescope. In order to estimate the parallax effects on the microlensing light curves we make use of the following useful geometrical relations¹⁶

$$\begin{aligned}
 A_p &= \frac{u^2(t)+2}{u(t)\sqrt{u^2(t)+4}} \\
 u^2(t) &= p^2(t) + d^2(t) \\
 p(t) &= p_0(t) + \cos \psi [x_1(t) - x_1(t_0)] + \sin \psi [x_2(t) - x_2(t_0)] \\
 d(t) &= d_0 - \sin \psi [x_1(t) - x_1(t_0)] + \cos \psi [x_2(t) - x_2(t_0)] \quad , \quad (15) \\
 x_1(t) &= \rho [-\sin \chi \cos \phi (\cos \xi(t) - \epsilon) - \sin \chi \sin \phi \sqrt{1 - \epsilon^2} \sin \xi(t)] \\
 x_2(t) &= \rho [-\sin \phi (\cos \xi(t) - \epsilon) + \cos \phi \sqrt{1 - \epsilon^2} \sin \xi(t)] \\
 \rho &= \frac{a_{\oplus}(1-x)}{R_E} \quad p_0(t) = \frac{(t-t_0)}{T_E} \quad d_0 = u_0
 \end{aligned}$$

where $\xi(t)$ is implicitly given by

$$t = \sqrt{\frac{a_{\oplus}^3}{GM_{\odot}}} (\xi - \epsilon \sin \xi). \quad (16)$$

Here, a_{\oplus} is the semi-major axis of the Earth orbit around the Sun, $\epsilon = 0.0167$ is the Earth orbit eccentricity and ρ is the length of the semi-major axis projected onto the lens plane measured in Einstein radii. The position of the source stars is characterized by the parameters ϕ , χ and ψ in the relations (15) which give, respectively, the longitude measured in the ecliptic plane from perihelion towards the Earth motion, the latitude measured from the ecliptic plane towards the northern point of the ecliptic and the rotation angle in the lens plane which describes the relative orientation of velocity v_T to the sun-earth system. We find that the deviations on the microlensing light curve due to the parallax effect depend substantially on the Earth position in its orbit at the time of the maximum amplification and get the largest value when $\xi_0 = 165^\circ$ that happens in June.

In the following calculations, we have assumed that the Euclid satellite is in the best position in its orbit in order to maximize the parallax effect on the microlensing event light curves. Using the usual transformation relations between coordinate systems, we find the following values for the Euclid's line of sight towards the Galactic bulge: $\phi \simeq 167.8^\circ$ and $\chi \simeq -5.4^\circ$.

To the aim of estimating the number of events for which the parallax feature affects the microlensing light curves as observed by Euclid, we make use of Monte Carlo numerical simulations by generating microlensing events towards the field of the sky planned to be observed by the Euclid telescope. Here, we briefly describe the adopted strategy. In particular, we draw

- a) lens distances D_l , based on the above written disk or bulge spatial distributions. We always consider the source as being located in the Galactic bulge, so we fixed $D_s = 8.5$ kpc for all events;
- b) the relative transverse velocity from the velocity distribution;
- c) the impact parameter randomly distributed on a uniform interval $[0, 6.54]$. As already anticipated, the Euclid amplification threshold is planned to be $A_{th} = 1.001$;
- d) the lens mass that follows the mass function distribution in eq. (6).

In each case we choose the same position of the Earth, $\xi_0 = 165^\circ$, at the time t_0 of the light curve peak amplification.

The parallax effect is estimated by calculating the residuals between the light curve $A_p(t)$ containing the parallax effect from eqs. (15) and the corresponding standard curve $A_s(t)$ (3), i.e. $Res = |A_s(t) - A_p(t)|$. As an example, in Fig.1 we show the standard curve, the parallax curve and residuals in the case of a free-floating planet with mass $10^{-3}M_\odot$ at distance $D_l = 4.5$ kpc from Earth. As one can see, in this case the residuals are up to $\simeq 12\%$.

5. Results

We have calculated the microlensing optical depth from eq. (12) and the microlensing rate from eq. (13) for all the lens populations towards the Galactic bulge: FFPs, BDs and stars distributed in the thin disk, thick disk and the Galactic bulge. For their spatial distribution we use eqs. (8), (9), (10), coupled with the mass functions (5) and (6). For stars we assume the Salpeter mass function $\frac{dN}{dM} \sim M^{-2.4}$, while the relation between α_{BD} and α_{PL} is defined by equation (7).

Brown dwarfs are faint objects distinguished only in Sun surroundings. Recently, the ratio R (in the Solar Neighbourhood) between the number of stars with mass in the range $[0.08, 1]M_\odot$ and BDs in the range $[0.03, 0.08]M_\odot$, has been estimated by ¹⁷. From Table 1 in ¹⁷ we adopt a mean value of $R \simeq 5.1$ and assume that it applies to the whole Galaxy.

In Table 1, we show the results of our calculations of the optical depth for FFPs and BDs considered as lenses. We perform separate calculations for each structure of the galaxy (bulge, thin disk and thick disk) and different values of α_{PL} . The number of FFPs per star is chosen following Sumi et al. ³: the lowest value

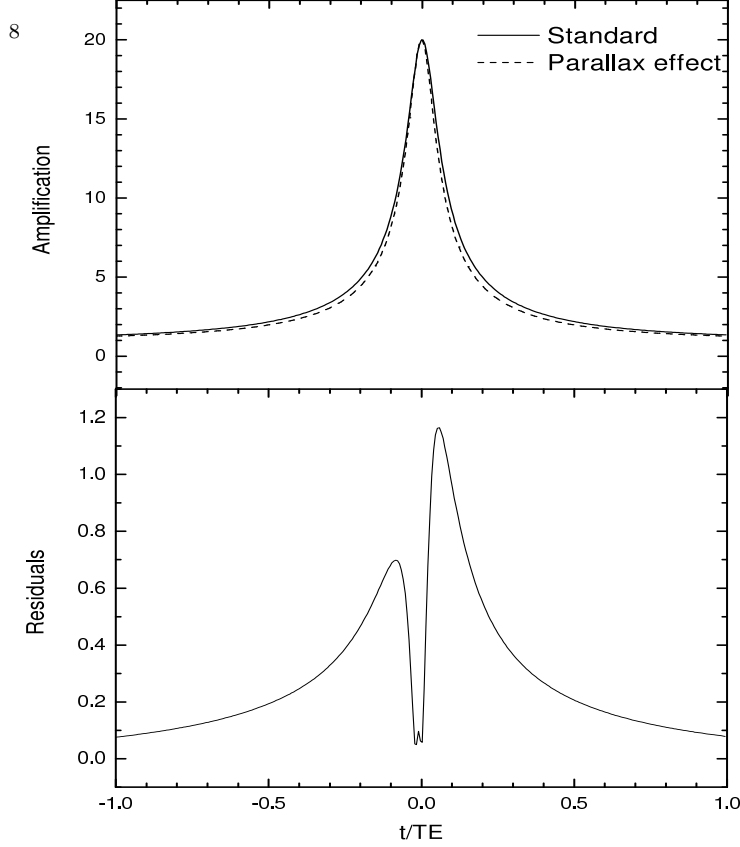


Fig. 1. Upper panel: the standard Paczyński light curve (continuous line) and the parallax curve (dashed line) for a planet with mass $10^{-3}M_{\odot}$ at distance $D_l = 4.5$ kpc from Earth are shown. The residual curve between the two curves is also shown (bottom panel).

$N_{PL} = 1.2$, mid value $N_{PL} = 5.5$ and highest value $N_{PL} = 23.6$. The optical depth yielded by stars is not dependent on α_{PL} : our calculations give 2.59×10^{-6} for bulge stars, 4.26×10^{-7} for thin disk stars and 2.42×10^{-7} for thick disk stars, respectively.

Table 1. Optical depth for FFPs and BDs, distributed in bulge, thin and thick disk, for different values of α_{PL} and for fixed values 23.6, 5.5 and 1.2 of the number of FFPs per star.

α_{PL}	$N_{PL} = 1.2$ ($\times 10^{-9}$)			$N_{PL} = 5.5$ ($\times 10^{-8}$)			$N_{PL} = 23.6$ ($\times 10^{-8}$)			BD ($\times 10^{-8}$)		
	<i>Blg</i>	<i>D_{thin}</i>	<i>D_{thc}</i>	<i>Blg</i>	<i>D_{thin}</i>	<i>D_{thc}</i>	<i>Blg</i>	<i>D_{thin}</i>	<i>D_{thc}</i>	<i>Blg</i>	<i>D_{thin}</i>	<i>D_{thc}</i>
0.9	22.1	3.52	2.00	10.1	1.61	0.92	43.4	6.92	3.93	9.95	1.59	0.90
1.0	17.6	2.80	1.59	8.04	1.28	0.73	34.5	5.51	3.12	10.0	1.60	0.91
1.1	13.5	2.16	1.22	6.19	0.99	0.56	26.5	4.24	2.40	10.1	1.61	0.92
1.2	10.1	1.62	0.92	4.64	0.74	0.42	19.3	3.19	1.81	10.1	1.63	0.92
1.3	7.43	1.18	0.67	3.40	0.54	0.31	14.6	2.32	1.32	10.3	1.64	0.93
1.4	5.36	0.86	0.49	2.46	0.39	0.22	10.5	1.68	0.95	10.3	1.65	0.93
1.5	3.84	0.61	0.35	1.76	0.28	0.16	7.54	1.21	0.68	10.4	1.67	0.94
1.6	2.74	0.48	0.25	1.26	0.20	0.12	5.40	0.86	0.49	10.4	1.68	0.95

We remark that the contribution of the bulge populations in the optical depth

is the most important one.

In Table 2, we show the results of our calculations for the microlensing rate (the probability to have a microlensing event per star during the observation time of one month), in the same conditions as above. The microlensing rate by stars is of course independent on α_{PL} , its value being 2.41×10^{-6} for bulge stars, 1.27×10^{-7} for thin disk stars and 1.69×10^{-7} for thick disk stars, respectively.

Table 2. Microlensing rate (the probability to have a microlensing event per star during the observation time of one month) for FFPs and BDs, distributed in bulge, thin and thick disk, for different values of α_{PL} and for fixed values $N_{PL} = 1.2, 5.5$ and 23.6 of the number of FFPs per star.

α_{PL}	$N_{PL} = 1.2$ ($\times 10^{-8}$)			$N_{PL} = 5.5$ ($\times 10^{-8}$)			$N_{PL} = 23.6$ ($\times 10^{-7}$)			BD ($\times 10^{-8}$)		
	Blg	D_{thin}	D_{thc}	Blg	D_{thin}	D_{thc}	Blg	D_{thin}	D_{thc}	Blg	D_{thin}	D_{thc}
0.9	21.7	1.14	0.91	93.3	5.23	4.18	42.6	2.25	1.79	23.3	1.24	1.66
1.0	18.5	0.98	0.78	84.7	4.47	3.56	36.3	1.92	1.53	23.6	1.25	1.66
1.1	15.5	0.82	0.65	71.0	3.75	2.99	30.5	1.61	1.28	23.7	1.25	1.67
1.2	12.9	0.68	0.54	59.0	3.12	2.49	25.3	1.34	1.07	23.7	1.26	1.67
1.3	10.7	0.56	0.45	48.8	2.59	2.05	20.9	1.11	0.88	23.9	1.26	1.68
1.4	8.95	0.47	0.37	40.6	2.14	1.71	17.4	0.92	0.73	24.0	1.27	1.69
1.5	7.43	0.39	0.31	34.1	1.80	1.43	14.6	0.78	0.62	24.1	1.27	1.69
1.6	6.33	0.34	0.27	29.0	1.54	1.22	12.5	0.66	0.53	24.2	1.28	1.70

The dominant contribution in the microlensing rate is again that of the bulge lens populations. We then estimate the number of microlensing events expected to be detectable by the Euclid telescope (taking $A_{th} = 1.001$ and therefore $u_{max} = 6.54$) multiplying the microlensing event rate by the number of source stars in the Euclid field of view $N_{ED} = 2.3 \times 10^8$ and by the observation time duration.

In Table 3, we show the results of our calculations for the estimated number of microlensing events per month, where FFPs and BDs are considered as lenses. We perform separate calculations for each structure of the galaxy: bulge, thin disk and thick disk. The number of microlensing events per month produced by stars is not dependent on α_{PL} , its value is 3657 for bulge stars, 193 for thin disk stars and 265 for thick disk stars.

Table 3. Number of microlensing events detectable by the Euclid telescope in one month of observation towards the Galactic bulge for the different lens populations and for different values of α_{PL} .

α_{PL}	$N_{PL} = 1.2$			$N_{PL} = 5.5$			$N_{PL} = 23.6$			BD		
	Blg	D_{thin}	D_{thc}	Blg	D_{thin}	D_{thc}	Blg	D_{thin}	D_{thc}	Blg	D_{thin}	D_{thc}
0.9	328	17	14	1505	79	63	6457	340	272	354	19	25
1.0	280	15	12	1284	68	54	5507	291	232	358	19	25
1.1	235	12	10	1077	57	45	4603	244	195	359	19	25
1.2	195	10	8	894	47	38	3838	203	162	359	19	25
1.3	161	9	7	740	39	31	3175	168	134	362	19	26
1.4	134	7	6	615	33	26	2638	139	111	363	19	26
1.5	113	6	5	516	27	22	2215	117	93	365	19	26
1.6	96	5	4	440	23	19	1888	100	80	366	19	26

The bulge population contribution is the most important one also in this case.

In Fig.2 we present our estimations for the total number of microlensing events due to BDs and FFPs per month, for different values of α_{PL} .

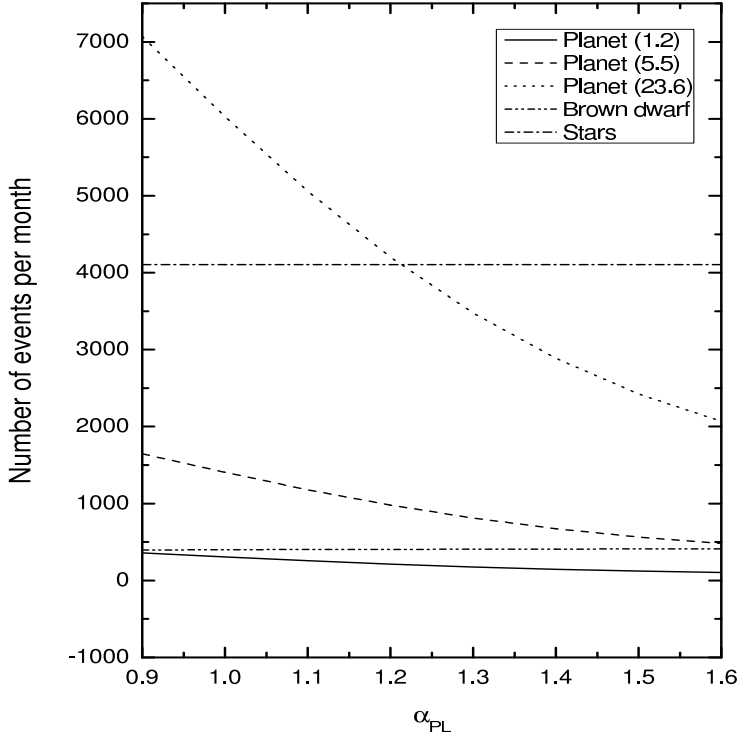


Fig. 2. The total microlensing event number due to BDs (dot-dot-dashed line), stars (dot-dashed line) and FFPs expected to be detectable in one month of observation towards the Galactic bulge by the Euclid telescope as a function of α_{PL} . The three curves for the FFP contribution are drawn assuming $N_{PL} = 5.5$ (dashed line), $N_{PL} = 23.6$ (dotted line), $N_{PL} = 1.2$ (continuous line).

By numerical simulations we produce a large number of microlensing events caused by the population of the FFPs. We assume that a microlensing event can be detected if in its light curve there are at least 8 points in which the amplification is bigger than the threshold amplification $A_{th} = 1.001$. The photometric error in this case is 0.1%

$$A_{th}F - F = F(A_{th} - 1) = \Delta F \Rightarrow (A_{th} - 1) = \frac{\Delta F}{F} = 1.001 - 1 = 0.001. \quad (17)$$

In the case of Euclid telescope, the expected curve will contain points determined every 20 minutes, that means that any detectable event has to have a duration larger than 2.67 hours.

For estimating the parallax effect on the observed light curves, we consider only

those containing at least 8 points with $Res > 0.001$ inside Einstein ring

$$|A_s(t)F - A_p(t)F| > \Delta F \Rightarrow |A_s(t) - A_p(t)| > \frac{\Delta F}{F} \Rightarrow Res > 0.001. \quad (18)$$

We retain all synthetic events with residuals fulfilling the above-mentioned condition. Therefore, the efficiency for parallax effect detection is given by the ratio between the number of these events and the total number of detectable events.

In Fig.3 we show our results for the parallax efficiency in microlensing events caused by FFPs and expected to be detectable by Euclid are shown. We consider three separate distributions, bulge, thin and thick disk lenses and show the parallax efficiency with respect to the value of α_{PL} .

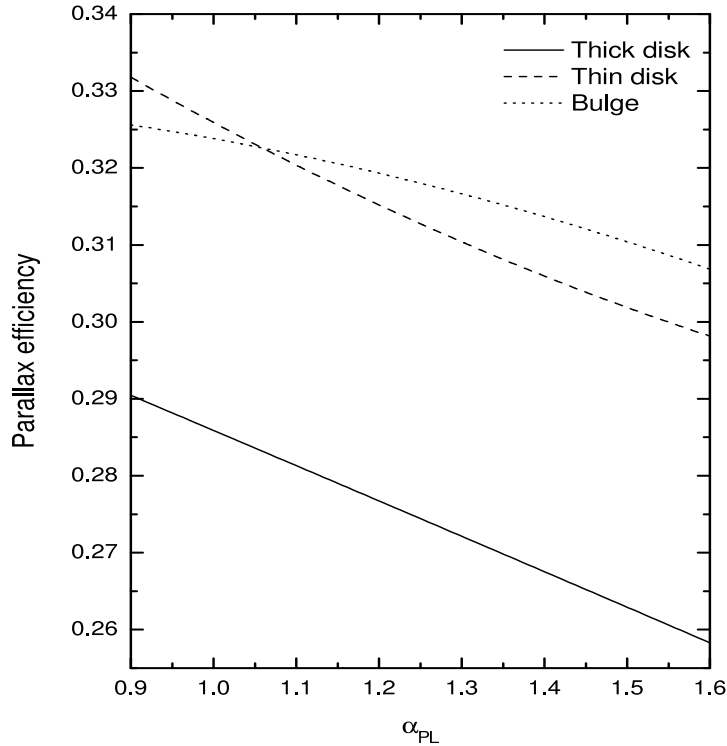


Fig. 3. Parallax efficiency caused by free-floating planets as a function of α_{PL} for the three different distributions of FFPs: bulge FFPs (dotted line), thin disk FFPs (dashed line) and thick disk FFPs (continuous line).

For example, as one can see, in the case of $\alpha_{PL} = 1.3$ the parallax efficiency caused by bulge FFPs is 32%, by thin disk FFPs is 31% and by thick disk FFPs is 27%. So, approximately in 30% of the detectable events, the parallax effect due to the Earth motion may be detectable by the Euclid telescope, allowing to partially

resolve the parameter degeneracy problem in this kind of observations and constrain the distance to the FFPs. This should allow to estimate not only the number of FFPs throughout the Milky Way, but also their spatial distribution.

6. Conclusions

In this paper we investigate the possible observation of free-floating planets (in addition to normal stars and brown dwarfs) towards the Galactic bulge by the future Euclid space-based observatory, via detection of microlensing light curves. These events, either considered statistically or individually, are an important base of knowledge to better characterize the galactic populations of objects in addition to normal stars.

For the calculation of the optical depth and the microlensing rate for brown dwarfs we assume that they are distributed like stars, spatially and in the velocity space. This should also be true for free-floating planets, based on the idea that these objects are most likely formed in proto-planetary disks and subsequently scattered into unbound or very distant orbits. The number of these objects per star is poorly constrained, as is also the slope of their mass distribution.

We find that the optical depth and the microlensing rate for FFPs towards the Galactic bulge are much smaller than for stars, but slightly higher than for brown dwarfs. The highest contribution for the three object populations always comes from bulge objects. The theoretical optical depth and microlensing rate depend on the power law index of the FFP mass function, hence the corresponding observed values can be considered as sources of information for the still largely unknown mass function of brown dwarfs and FFPs.

By theoretical calculations we predict that a considerably large number of microlensing events produced by free-floating planets towards the Galactic bulge are potentially observable by the Euclid satellite. We also take into account the deviations in the microlensing light curves due to FFPs induced by the Earth parallax effect. We find that these deviations depend substantially on the Earth position in its orbit around the Sun at the time of the event maximum amplification and get the largest value in June. By numerical simulations we also find that the efficiency (that is the ratio between the number of events due FFPs that fulfill equation (18) with respect to the total number of detectable events) of detecting the Earth parallax effect in the light curves due to FFPs is potentially interesting since the parallax effect turns out to be detectable in about 1/3 of all observable events (see Fig.3). We emphasize that the observation of this effect may allow to constrain the FFP distances, which is a fundamental information necessary to investigate how FFPs are distributed throughout the Milky Way. This, in turn, is an important issue in order to establish their origin.

As a final remark we caution that the short time-scale microlensing features, such as those expected due to the Earth parallax, may be confused due to the so-called red-noise effect. Indeed, photometric observations are generally affected by

the presence of the Earth atmosphere that is a source of correlated noise. A way to circumvent this problem is to use space-based telescopes, an opportunity that has clearly many advantages. However, the improved sensitivity of space-based observations have unveiled a new source of noise related to the intrinsic stellar variability that induces the red-noise, connected to the correlated time-series. This effect has been studied in connection to the transit technique when searching for exoplanets as observed by space telescopes such as CoRoT and Kepler^{18,19}. The detailed study of this effect in connection to the microlensing lightcurves, in particular in connection to the searches for free-floating planets, is left to a following work.

We would like to thank the colleagues who have discussed the subject of this paper with us and particularly Francesco De Paolis for guidance and useful comments.

References

1. B. Paczyński, *Astrophys. J.* **304** (1986) 1
2. M.C. Smith, S. Mao and B. Paczyński, *Month. Not. Royal Astron. Soc.* **339** (2003) 925
3. T. Sumi et al., *Nature* **437** (2011) 349
4. G. Gilmore, R.F.G. Wyse and K. Kuijken, *Astron. Astrophys.* **27** (1989) 555
5. F. De Paolis, G. Ingrosso and A. Nucita, *Astron. Astrophys.* **366** (2001) 1065
6. M. Hafizi, F. De Paolis, G. Ingrosso and A. Nucita, *Int. Journ. Mod. Phys. D* **13** (2004) 1831
7. E. Dwek et al., *Astrophys. J.* **445** (1995) 716
8. Ch. Han and A. Gould, *Astrophys. J.* **447** (1995) 53
9. Ch. Han and A. Gould, *Astrophys. J.* **467** (1996) 540
10. I. A. Bond et al., *Month. Not. Royal Astron. Soc.* **327** (2001) 868
11. T. Sumi et al., *Astrophys. J.* **636** (2006) 240
12. R. Laureijs et al., Euclid Mapping the geometry of the dark Universe, ESA/SRE (2011), arXiv:1110.3193v1
13. K. Griest, *Astrophys. J.* **366** (1991) 412
14. Ph. Jetzer Ph, L. Mancini, and G. Scarpetta, *Astron. Astrophys.* **393** (2002) 129
15. E.E. Salpeter, *Astrophys. J.* **121**, (1995) 161
16. M. Dominik, *Astron. Astrophys.* **329**(1998) 361
17. A. Parravano, C. McKee and D. Hollenbach, *Astrophys. J.* **726** (2011) 27
18. F. Pont, S. Zucker and Queloz, *Month. Not. Roy. Astron. Soc.* **373** (2006) 231
19. S. Carpano and M. Fridlund, *Astron. Astrophys.* **485** (2008) 607